INTERNATIONAL JOURNAL FOR NUMERICAL METHODS IN FLUIDS
Int. J. Numer. Meth. Fluids 2008; **56**:2069–2090
Published online 25 September 2007 in Wiley InterScience (www.interscience.wiley.com). DOI: 10.1002/fld.1607

A method to discretize non-planar fractures for 3D subsurface flow and transport simulations

Thomas Graf*, †, ‡ and René Therrien

Département de Géologie et Génie Géologique, Université Laval, Ste-Foy, Qué., Canada G1K 7P4

SUMMARY

A method is presented to discretize inclined non-planar 2D fractures within a 3D finite element grid for subsurface flow and transport simulations. Each 2D fracture is represented as a triangulated surface. Each triangle is then discretized by 2D fracture elements that can be horizontal, vertical or inclined and that can be triangular or rectangular. The 3D grid representing a porous rock formation consists of hexahedra and can be irregular to allow grid refinement. An inclined fracture was discretized by (a) inclined triangles and (b) orthogonal rectangles and flow/transport simulations were run to compare the results. The comparison showed that (i) inclined fracture elements must be used to simulate 2D transient flow, (ii) results of 2D/3D steady-state and 3D transient flow simulations are identical for both discretization methods, (iii) inclined fracture elements must be used to simulate 2D/3D transport because orthogonal fracture elements significantly underestimate concentrations, and (iv) orthogonal elements can be used to simulate 2D/3D transport if fracture permeability is corrected and multiplied by the ratio of fracture surface areas (orthogonal to inclined). Groundwater flow at a potential site for long-term disposal of spent nuclear fuel was simulated where a complex 3D fracture network was discretized with this technique. The large-scale simulation demonstrates that the proposed discretization procedure offers new possibilities to simulate flow and transport in complex 3D fracture networks. The new procedure has the further advantage that the same grid can be used for different realizations of a fracture network model with no need to regenerate the grid. Copyright © 2007 John Wiley & Sons, Ltd.

Received 20 March 2007; Revised 11 July 2007; Accepted 21 July 2007

KEY WORDS: numerical model; fracture; discretization; 2D/3D; orthogonal grid

*Correspondence to: Thomas Graf, Département de Géologie et Génie Géologique, Université Laval, Ste-Foy, Qué., Canada G1K 7P4.
†E-mail: thomas.graf@geo.uni-goettingen.de
‡Now at the Center of Geosciences, Georg-August-University Göttingen, Goldschmidtstraße 3, 37077 Göttingen, Germany.

Contract/grant sponsor: Ontario Power Generation (OPG)
Contract/grant sponsor: Natural Sciences and Engineering Research Council of Canada (NSERC)

1. INTRODUCTION

Fractures in rock formations have a significant impact on groundwater flow and solute transport. For example, fractures represent preferential pathways where solutes migrate at velocities that are several orders of magnitude larger than within the rock matrix itself. Discrete fracture models have been used for theoretical and practical studies of fluid flow and solute transport [1–21]. Discrete fracture models are attractive because fracture network characteristics (e.g. fracture size, orientation and aperture) reflect the physical properties of the rock, hence making it possible to investigate different network parameters and to quantify stochastic uncertainty associated with fracture networks [7]. There are, however, some limitations to the practical application of the discrete fracture approach. For example, the geometry of complex fracture networks within a permeable matrix is difficult to represent in a numerical grid. Although natural fracture surfaces probably resemble non-planar polygons, the geometry of these surfaces is often simplified and represented by one-dimensional segments [2, 12, 16, 18], planar discs [1, 3, 7], planar rectangles [9, 14, 19–21] or planar polygons [11, 18]. While these simplifications can be adequate for conceptual studies, investigating a real system requires that the fracture network be represented in the grid in its full complexity.

Because the exact location and geometry of real fractures are difficult to determine, fracture network characteristics such as fracture shape, orientation, and connectedness are often assumed to obey geostatistical distributions [22–26]. Therefore, stochastic approaches are very common to generate fracture networks and to capture uncertainty in the knowledge of fractures [2, 3, 7, 12, 27–29]. For example, in a stochastic Monte-Carlo approach, numerous realizations of fracture networks are generated and the result of flow and transport simulations from all networks are averaged. The number of networks generated is considered sufficient when the averaged result remains unchanged if additional realizations are produced. Because the number of realizations required is usually high (>100), the geometry of each fracture network should be efficiently imported into the grid to keep simulation times within reasonable limits.

Uncertainty associated with fracture networks has previously been addressed by converting discretely fractured rock to a continuum medium. In that case, individual fractures are not explicitly represented and porous matrix elements have the equivalent permeability of the fractured rock [27, 28]. However, a limitation of this approach is the weak coupling between real fracture geometry and hydraulic properties of the model. When hydraulic properties of the fractured rock are converted to a continuum medium, the detailed structure of the fractured rock is not accounted for and properties of the hydraulically equivalent system may be very different from fractured rock properties [7]. This difference is greater when fracture density in the rock is small and when few large fractures dominate groundwater flow. In addition, not all fracture data are needed when using the equivalent porous medium approach and important information may potentially be missing in the model.

Prior groundwater flow studies in discretely fractured media have used different approaches to represent the complex geometry of fractured rock. Some studies have assumed an impermeable matrix where flow takes place only within the fracture planes [3–5, 8, 13, 30–36]. Bruines [37] has made the further assumption that flow only takes place along the 1D intersections of 2D fracture planes. Assuming that an impermeable matrix simplifies fracture discretization because the matrix does not need to be discretized and 2D fractures represent the only model domain requiring discretization. However, while the low-permeability porous matrix can be neglected for

DOI: 10.1002/fld

groundwater flow studies, it cannot always be neglected for solute transport studies because of potentially high diffusive fluxes within the rock matrix.

Moenickes *et al.* [38] have proposed a '2.75D' mesh generation of discretely fractured media. Their method discretizes fractures by 2D elements and subdivides the low-permeability porous matrix into two regions: (i) a region far from fractures and (ii) a region near fractures. Steady-state conditions are assumed in the first region, making its representation in the grid unnecessary. Transient conditions are assumed in the second region and the porous matrix near the fractures is discretized either by 3D prisms or 3D hexahedra. The '2.75D' mesh proposed by Moenickes *et al.* [38] is, therefore, a skeleton of 3D matrix elements covering 2D fracture planes. On the one hand, the method proposed by Moenickes *et al.* [38] is very useful to simulate flow and transport in fractures and parts of the matrix. On the other hand, simulations of different stochastic realizations of a fracture network, for example using a Monte-Carlo approach, cannot be done within a reasonable time frame because each simulation requires time-consuming re-meshing of the '2.75D' domain.

Representing the rock matrix in 3D and discrete fractures in 2D complicates the realistic representation of 2D fractures in 3D finite element grids. When orthogonal grids are used, discrete fractures are usually aligned on grid faces, allowing only for representation of orthogonal fractures [14, 16, 39]. Watanabe and Takahashi [12] have previously discretized inclined fractures on orthogonal grids, for a vertical 2D slice, by combining horizontal and vertical 1D fracture elements (pipes) that connect element-centered nodes of adjoining 2D porous matrix elements. This approach has been extended to 3D by Graf and Therrien [19–21], who have included inclined 2D fracture elements (in addition to horizontal and vertical ones) in the discretization of inclined fractures in a 3D porous medium. However, the approach of Graf and Therrien is restricted to the discretization of inclined fractures that are (i) rectangular, (ii) planar and (iii) parallel to at least one coordinate axis. Normani *et al.* [40] have recently developed a technique to discretize 3D arbitrarily inclined non-planar triangulated fractures in orthogonal grids by combining horizontal and vertical rectangular fracture elements. Their method, however, increases the actual fracture surface area and can influence simulation results, for example by underestimating solute concentrations because flow paths are lengthened.

Non-orthogonal irregular grids containing prisms, tetrahedra or distorted hexahedra can also be used to discretize fractures in 3D. In that case, the grid geometry must be chosen such that face locations of 3D porous matrix elements coincide with locations of 2D fractures [18, 41, 42]. That method has the disadvantage that discretizing fracture networks of high complexity is very challenging, time consuming and sometimes impossible. Describing discrete fractures within an irregular 3D grid is further complicated when fractures are non-planar.

The objective of this study is to develop a flexible method to discretize 2D fractures within a 3D porous matrix to address statistical uncertainty associated with fluid flow and solute transport in fractured rock. We introduce a new technique to discretize non-planar inclined discrete fractures, developed with the FRAC3DVS model, which solves 3D flow and solute transport in discretely fractured porous media [14]. The enhanced model triangulates non-planar inclined fractures and represents each triangle by a series of rectangular and triangular fracture elements, which can be horizontal, vertical or inclined. With the improved model, we discretize a single inclined fracture and conduct flow/transport simulations in 2D and 3D. The results are compared with simulations where the inclined fracture is represented by orthogonal elements. Finally, we present an application of the model to simulate field-scale fluid flow in a fractured granitic rock formation.

DOI: 10.1002/fld

2. NUMERICAL MODEL

FRAC3DVS is a 3D variable-density saturated–unsaturated numerical groundwater flow and multi-component solute transport model, which represents fractures using either the discrete fracture approach or an equivalent porous medium approach. The governing equations for flow and solute transport are identical to those used by Graf and Therrien [19]. A detailed description of the model can be found elsewhere [14, 19–21, 43] and is not repeated here. The following section focuses on the modification of the FRAC3DVS model to discretize inclined non-planar discrete 2D fractures within a 3D orthogonal finite element grid.

2.1. Model development

Discretizing non-planar 2D fractures in a 3D orthogonal grid comprises the following steps, which will be discussed in further detail below:

(1) Triangulate a non-planar natural fracture by a series of planar triangles.
(2) Generate a 3D finite element grid using hexahedral elements.
(3) Find intersections of all triangles with the element edges.
(4) Move the element edge intersections to closest nodes. These nodes will ultimately become fracture nodes.
(5) Choose the 2D fracture elements (triangles and rectangles) that connect the fracture nodes for each 3D matrix element.
(6) Formulate derivatives of approximation functions of triangular fracture elements to solve for fluid flow and solute transport.

2.1.1. Step 1: Triangulate non-planar natural fractures. Triangulation is probably the most common approach to represent natural fractures in 3D because the fracture surfaces can be triangular, rectangular, disc-like, polygonal, planar or non-planar. A triangulated fracture surface consists of planar triangles as shown in Figure 1. Intersections of fractures with individual boreholes can be triangle apexes when triangulating natural fractures. The associated triangles are linear interpolation surfaces between borehole intersections with fractures. Geostatistical software such as FXSIM3D generates stochastic networks of triangulated fracture surfaces [44]. The number of triangles used to represent a real fracture depends on the modeler's judgement. Too few triangles represent a real fracture too roughly but too many triangles may complicate fracture discretization.

2.1.2. Step 2: Generate 3D finite element grid. A 3D grid with hexahedral elements is generated. Grid spacing need not be uniform and grid line density may be larger near a pumping well. The grid lateral boundaries need not be rectangular, for example to represent irregular horizontal boundaries, and the grid may contain distorted hexahedral elements to represent inclined geological strata or irregular domain topography. Figure 2 shows a distorted hexahedral element, where 4-node element faces on the domain top or bottom may be inclined. The figure also shows the 12 element edges of a hexahedral element. Note that the element edges need not be horizontal or vertical.

2.1.3. Step 3: Find element edge intersections. Element edge intersections are defined here as the points where an element edge intersects a fracture triangle. Intersections with all element edges are found with the equation of a planar fracture triangle, $ax + by + cz + d = 0$, and with the equation

DOI: 10.1002/fld

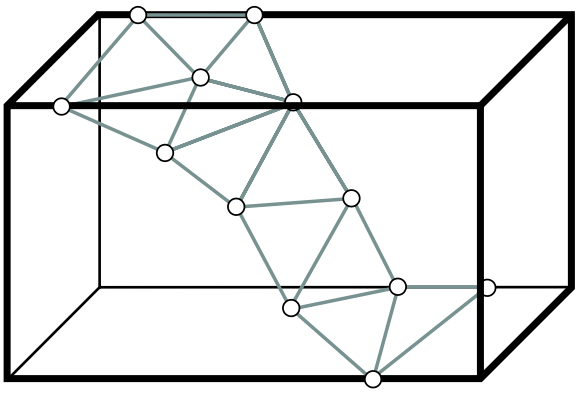

Figure 1. Representation of a non-planar fracture by a set of planar triangles. The intersection of the fracture with investigation boreholes is represented by hollow dots.

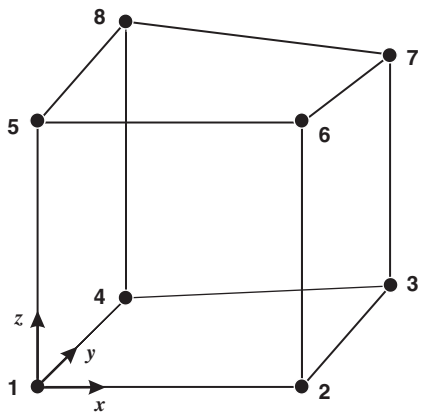

Figure 2. Element edges and local node numbering of a distorted 3D hexahedral porous matrix element.

of a straight element edge, $\boldsymbol{\omega} = \mathbf{OS}_1 + \lambda \cdot \mathbf{S}_1\mathbf{S}_2$, where $\boldsymbol{\omega}$ represents the element edge in vectorial form, O is the origin, S_1 and S_2 are start and end points of a segment and λ is a real number. Finally, a series of intersections with element edges is obtained. Figure 3(a) shows element edge intersections with a single triangle. Note that, for clarity, the figure only shows the intersections on the left front boundary of the cubic model domain.

2.1.4. Step 4: Move intersections to closest nodes. Step 4 identifies nodes that can become fracture nodes and also generates a list of possible fracture nodes for each 3D finite element. The element edge intersections found in the previous step do not necessarily correspond to a node of the finite element grid. Because the objective is to represent complex fracture networks on easily generated grids, the element edge intersections are moved to the closest grid nodes, such that the original finite element grid geometry is retained (Figure 3(b)). For each 3D porous matrix element, the distances from local nodes 1–8 (Figure 2) to the intersection are compared and the intersection is moved to the closest node.

DOI: 10.1002/fld

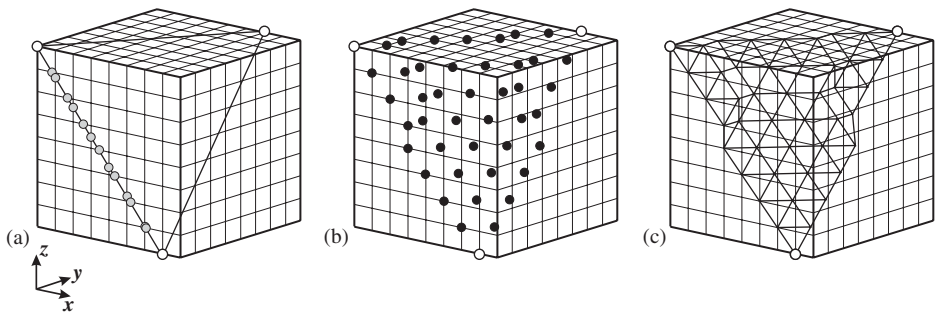

Figure 3. Discretization of a planar fracture triangle: (a) find intersections of the triangle with element edges, shown by grey dots; (b) move element edge intersections to closest nodes, shown by black dots; and (c) select 2D fracture elements from selected nodes.

When an intersection is located at the same distance to two nodes, node numbering of the finite element grid will control the node to which the intersection is moved. The intersection will always be moved to the node with the lower number. For example, if an intersection is located exactly between local nodes 2 and 6 (Figure 2), the intersection will be moved to node 2 because node 6 is not closer to the intersection. However, if an intersection is exactly between nodes 1 and 2, it is moved to node 1. It should be noted that some intersections may be moved to the same node.

2.1.5. Step 5: Choose triangular and rectangular fracture elements. Between 0 and 7 fracture nodes are assigned to each 3D hexahedral element in step 4. Step 5 finds the 2D fracture element(s) (triangles and/or rectangles) that connect the assigned fracture nodes in each 3D matrix element. Choosing fracture elements from assigned fracture nodes is governed by the rules shown in Table I where local node numbers are used (Figure 2). These rules have been defined (i) to ensure that the orientation of the chosen fracture elements reflects the natural fracture orientation, (ii) to minimize the surface of the discretized fracture with respect to the surface of original triangulated fracture plane and (iii) to guarantee that most segments forming the edges of the 2D fracture elements are located on an outer surface of 3D matrix elements. The rules imply that not all potential fracture nodes may be included in one of the chosen fracture elements. For example, in case 7 (Table I), the global fracture orientation is probably best represented by choosing triangle 1–3–6 as a fracture element. In that case, node 2 is dropped because choosing triangles 1–2–3, 1–2–6 and 2–3–6 increases the fracture surface area with respect to the natural fracture and it does not maintain the natural fracture orientation. Rule (iii) guarantees continuity of fracture surface and avoids creation of artificial holes in the discretized fracture. For example, in case 6, choosing triangles 1–2–5 and 2–3–5 represents the natural fracture orientation equally well as choosing 1–2–3 and 1–2–5 but, in the former case, the outer segment 1–3 is inexistent. Furthermore, a third fracture element which would be located in the matrix element underneath and which would contain segment 5–7 would not connect to either 1–2–5 or 2–3–5, hence creating an artificial hole in the fracture surface between nodes 1–2–3.

The result of step 5 is a fully connected fracture that is discretized by 2D horizontal/vertical/inclined triangular/rectangular fracture elements. Figure 3(c) shows the discretized continuous fracture of Figure 3(a).

DOI: 10.1002/fld

Table I. Rules to choose fracture elements (triangles △ and/or rectangles □) from selected fracture nodes.

Case	Number of fracture nodes	Fracture nodes selected	Fracture element(s) chosen
1	0	None	None
2	1	Any node	None
3	2	Any 2 nodes	None
4	3	Any 3 nodes	△ Through the 3 nodes
5	4	Any 4 nodes on a plane	□ Through the 4 nodes
6	4	1–2–3–5	△1–2–3 and △1–2–5
7	4	1–2–3–6	△1–3–6
8	4	1–2–3–8	△1–2–3 and △1–3–8
9	5	1–2–3–4–5	□1–2–3–4
10	5	1–2–3–5–7	△1–2–5 and △2–3–7 and △2–5–7
11	5	1–2–3–5–8	△1–2–3 and △1–3–8 and △1–5–8
12	6	1–2–3–4–5–6	□1–2–3–4 and □1–2–5–6
13	7	1–2–3–4–5–6–7	□1–2–3–4 and □1–2–5–6 and □2–3–6–7

The method can be used to discretize fractures obtained from different realizations with the same grid as shown in Figure 4 where two simple irregular fractures are discretized. The fracture in each realization is triangulated by the eight planar triangles shown on the left in Figure 4, and the two examples could be regarded as two stochastic realizations of the same fracture. The orthogonal grid (not shown) is refined near a vertical borehole, located in the domain center. Clearly, the same grid is used for the two realizations and it does not have to be adapted and rebuilt for each realization. This is a great advantage of the method presented here. Thus, the proposed discretization method is a time saving and flexible way to represent multiple realizations of a fracture network model for irregular grids. Therefore, performing a large number of numerical simulations using different stochastic fracture network realization is not limited by the time required to construct complex grids for each realization. Figure 4 also shows that the proposed discretization method works well for a grid with non-uniform grid line spacing.

2.1.6. Step 6: Formulate derivatives of approximation functions. Derivatives of approximation functions need to be formulated for the inclined triangular fracture elements. The derivatives account for any shape and orientation of triangular elements. Approximation functions are formulated within a Cartesian coordinate system using the local coordinates $\overline{x}$ and $\overline{y}$. If the local coordinates of node i are $(\overline{x}_i, \overline{y}_i)$ and if node 1 is at the origin of the local coordinate system, derivatives of approximation functions (N_i) can be written as [45]

$$\frac{\partial N_1}{\partial \overline{x}} = \frac{\overline{y}_2 - \overline{y}_3}{2A}, \quad \frac{\partial N_1}{\partial \overline{y}} = \frac{\overline{x}_3 - \overline{x}_2}{2A}$$

$$\frac{\partial N_2}{\partial \overline{x}} = \frac{\overline{y}_3}{2A}, \quad \frac{\partial N_2}{\partial \overline{y}} = -\frac{\overline{x}_3}{2A} \tag{1}$$

$$\frac{\partial N_3}{\partial \overline{x}} = -\frac{\overline{y}_2}{2A}, \quad \frac{\partial N_3}{\partial \overline{y}} = \frac{\overline{x}_2}{2A}$$

DOI: 10.1002/fld

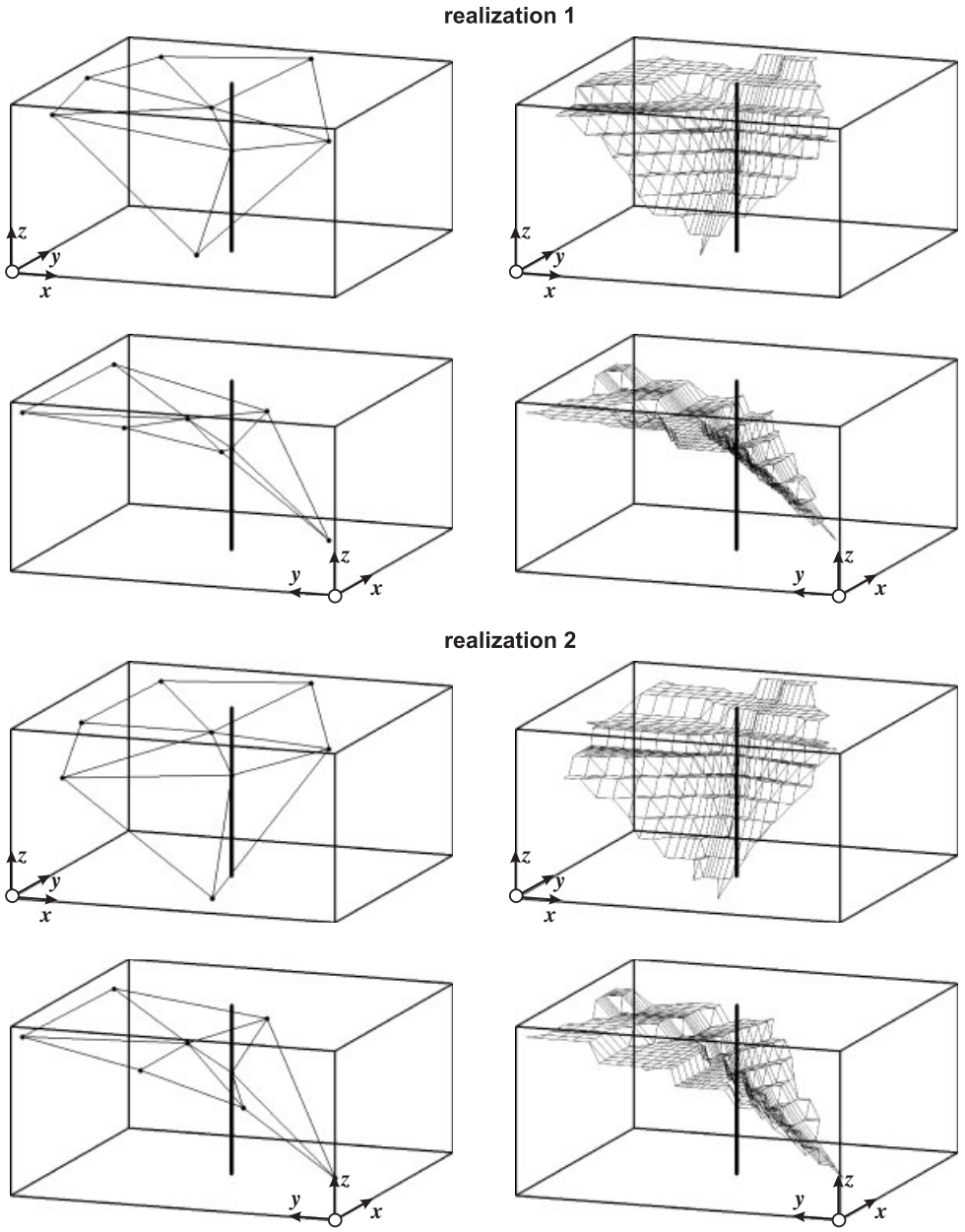

Figure 4. Discretization of two realizations of a non-planar fracture in an irregular finite element grid containing a vertical borehole. Two perspectives of the triangulated fracture (left) and its discretized form (right) are shown.

DOI: 10.1002/fld

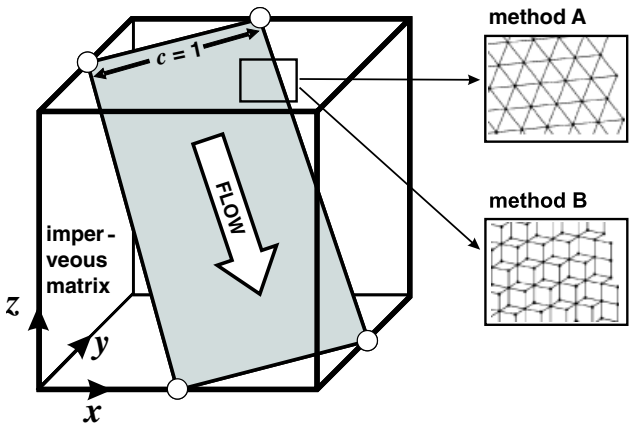

Figure 5. Model design for test case 1 and for further 3D simulations. The inclined fracture has been discretized by inclined triangles (method A; this study) and orthogonal rectangles (method B, [40]).

where $A(L^2)$ is the surface area of the triangular element. The model applies the control volume finite element method to the flow equation [14] and the Galerkin finite element method to the transport equation [19], with the derivatives of approximation functions as given by Equation (1).

2.2. Alternate discretization method of inclined fractures in 3D

Figure 5 shows an inclined fracture that was discretized with (i) inclined triangular elements using the method described in the previous section (referred to as method A) and (ii) and by selecting a series of horizontal and vertical rectangular 2D elements as developed by Normani *et al.* [40] (method B). Method B is computationally faster than method A, but it has the disadvantage that flow and transport paths can be significantly longer for the discretized fractures compared with the natural fracture.

2.3. Model verification

Two test cases to verify solute transport in fractured rock are presented. Case 1 verifies the new approximation functions for irregular triangular elements presented in Section 2.1.6 and Equation (1). While case 1 focuses on flow and transport only in a fracture and neglects the presence of the rock matrix, test case 2 verifies flow and transport in a fracture embedded in a low-permeability porous matrix.

2.3.1. Case 1: solute transport in an inclined fracture embedded in an impermeable matrix. The model domain for the first test case is a cube with a side length of 10 m and consists of 216 000 hexahedral elements of side length 0.1667 m (Figure 5). The cubic domain is considered impermeable, except for a single fracture that is discretized with 3540 equilateral triangles (method A) of side length 0.2357 m. Fluid flow and solute transport parameters are identical to those used by Shikaze *et al.* [16] and are listed in Table II. The lateral boundaries of the fracture are impermeable and the top and bottom boundaries of the fracture are assigned constant hydraulic heads to create a uniform flow field with velocity $v = 1.484 \times 10^{-3}\,\mathrm{m\,s^{-1}}$. The top boundary of the fracture is

DOI: 10.1002/fld

Table II. Model parameters used for the analysis of flow and solute transport in 2D and 3D.

Parameter	Value
Free-solution diffusion coefficient (D_d)	$5 \times 10^{-9}\,m^2\,s^{-1}$
Water density (ρ_0)	$1000\,kg\,m^{-3}$
Water viscosity (μ)	$1.1 \times 10^{-3}\,kg\,m^{-1}\,s^{-1}$
Specific storage of matrix (S_S)	$9.96 \times 10^{-5}\,m^{-1}$
Matrix permeability (κ_{ij})	$10^{-15}\,m^2$
Matrix longitudinal dispersivity (α_l)	0.1 m
Matrix transverse dispersivity (α_t)	0.005 m
Matrix porosity (ϕ)	0.35
Tortuosity (τ)	0.1
Specific storage of fracture (S_S^{fr})	$4.32 \times 10^{-6}\,m^{-1}$
Fracture dispersivity (α^{fr})	0.1 m
Fracture aperture ($2b$)	50 μm

All parameter values are identical to those used by Shikaze *et al*. [16]. The mathematical symbols correspond to those used by Graf and Therrien [19].

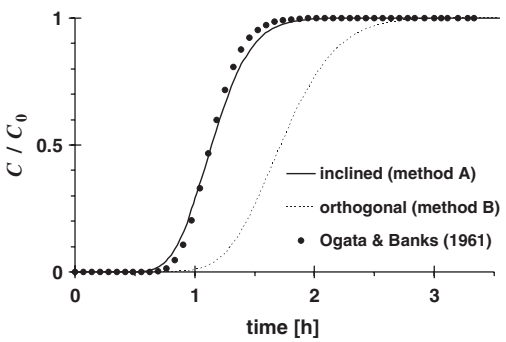

Figure 6. Concentration breakthrough curve of solute transport in an inclined fracture within an impermeable matrix. The analytical [46] and two numerical (FRAC3DVS) solutions using inclined (method A) and orthogonal (method B) fracture elements are shown.

assigned a constant solute source of relative concentration $c = 1$. The described fracture boundary conditions are chosen to force 1D advective–dispersive–diffusive solute transport in the fracture, allowing comparison with the Ogata–Banks [46] analytical solution. Figure 6 shows that there is very good agreement between the analytical and numerical solutions using method A.

Figure 6 also shows the simulated concentration breakthrough curve for the inclined fracture discretized with orthogonal elements (method B). Concentrations are underestimated when using orthogonal elements. This discrepancy can be attributed to the longer transport path for method B compared with method A, which delays the arrival of the solute.

2.3.2. Case 2: solute transport in a fracture embedded in a porous matrix. In case 2, we used the analytical solution of solute transport for a single fracture in a porous matrix presented by Tang *et al*. [47]. Case 2 simulates advection in the single fracture, molecular diffusion and radioactive decay in both fracture and matrix and fracture–matrix diffusion in a transient regime. The model

DOI: 10.1002/fld

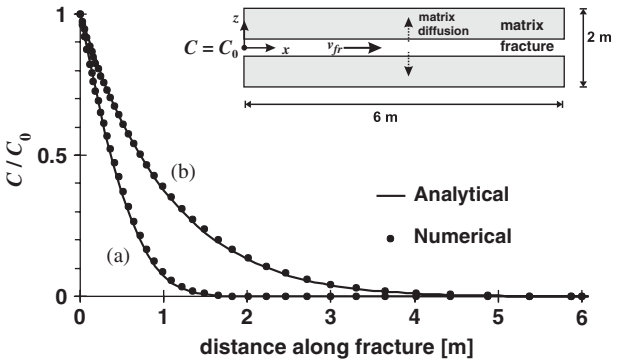

Figure 7. Concentration profiles of solute transport in a fracture within a low-permeability porous matrix. The figure shows concentrations at (a) 1000 days and (b) 10 000 days obtained from the analytical solution [47] and the numerical FRAC3DVS model.

Table III. Model parameters used to verify solute transport in a fracture embedded in a porous low-permeability matrix.

Parameter	Value
Matrix porosity (ϕ)	0.01
Matrix tortuosity (τ)	0.1
Free-solution diffusion coefficient (D_d)	$5.04576 \times 10^{-2}\,m^2\,yr^{-1}$
Half-life of solute (Tritium) ($T_{1/2}$)	12.35 yr
Fracture dispersivity (α_{fr})	0.0 m
Fracture groundwater velocity (v_{fr})	$3.65\,m\,yr^{-1}$
Fracture aperture ($2b$)	100 μm

All parameters are identical to those used by Tang *et al.* [47].

domain is a vertical slice of unit thickness with dimensions $\ell_x = 6$ m and $\ell_z = 2$ m (Figure 7). The finite element grid consists of 4312 hexahedral elements of unit thickness. The element sizes vary from $\Delta x = 0.01$ m (near the left boundary) to $\Delta x = 0.5$ m (near the right boundary) and from $\Delta z = 0.001$ m (near the fracture) to $\Delta z = 0.1$ m (near the top and bottom boundaries). The slice contains a horizontal planar 2D fracture located at $z = 0$. The fracture was discretized using triangular 2D elements. No flow (or solute flux) boundary conditions are imposed on all boundaries except the left and right boundaries where specified heads are applied such that the groundwater flow velocity in the fracture is $3.65\,m\,yr^{-1}$ ($= 0.01\,m\,day^{-1}$). A specified concentration of 1.0 is imposed at $x, z = 0, 0$. Flow and transport parameters are identical to those used by Tang *et al.* [47] and are summarized in Table III. Figure 7 shows two concentration profiles along the fracture at different times. The figure demonstrates very good agreement between the analytical [47] and numerical (this model) solutions proving that the numerical model correctly simulates flow and transport in fractured porous media.

DOI: 10.1002/fld

3. SIMULATION OF FLOW AND SOLUTE TRANSPORT IN 2D AND 3D

This section compares results when an inclined fracture is discretized with inclined triangles (method A) and when it is discretized with orthogonal rectangles (method B). The goal of this comparison is to determine how an inclined fracture is best represented, with method A or B, for a specific simulation context (for example steady-state or transient conditions, flow or transport). Simulation parameters for the 2D and 3D simulations are shown in Table II and are held constant unless otherwise stated.

For the 2D simulations, the model domain is a vertical slice of unit thickness with dimensions $\ell_x = 10\,\text{m}$ and $\ell_z = 10\,\text{m}$ (Figure 8). The finite element grid consists of 2500 hexahedral elements of size $\Delta x = \Delta z = 0.2\,\text{m}$ and of unit thickness. The vertical slice contains an inclined planar 2D fracture whose location is shown in Figure 8. For the numerical simulations, the inclined fracture was discretized using (a) inclined rectangles (method A) and (b) orthogonal (horizontal and vertical) rectangles (method B). Simulated hydraulic heads and concentrations are reported for an observation node located at $x = 5\,\text{m}$, $z = 5\,\text{m}$, which corresponds to a fracture node for both methods.

For the 3D model, the domain is identical to that used for the verification simulation (Figure 5) with the exception that the porous matrix is permeable. The boundary conditions along the fracture edges are identical to those used for the verification simulation. The boundaries of the cube are zero-dispersive flux for transport and impermeable to groundwater flow. For the numerical simulations, the inclined fracture shown in Figure 5 was discretized using (a) inclined triangles (method A) and (b) orthogonal rectangles (method B). The node at $x = 5\,\text{m}$, $y = 5\,\text{m}$, $z = 5\,\text{m}$ is a fracture node for both methods and it was used to obtain and compare simulation results.

3.1. Flow simulations

Steady-state and transient flow simulations were conducted in 2D and 3D. Steady-state flow simulations show that the hydraulic head distribution for both discretization methods (A and B) is identical in 2D and 3D (results not shown). The initial condition for the transient simulations in 2D and 3D is $h_0(t = 0) = 0.0\,\text{m}$.

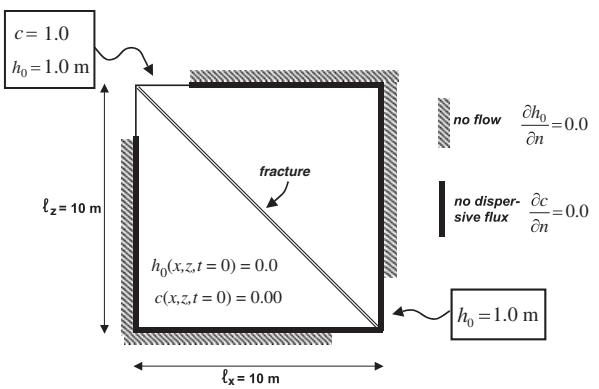

Figure 8. Simulation geometry, boundary and initial conditions for 2D simulations.

DOI: 10.1002/fld

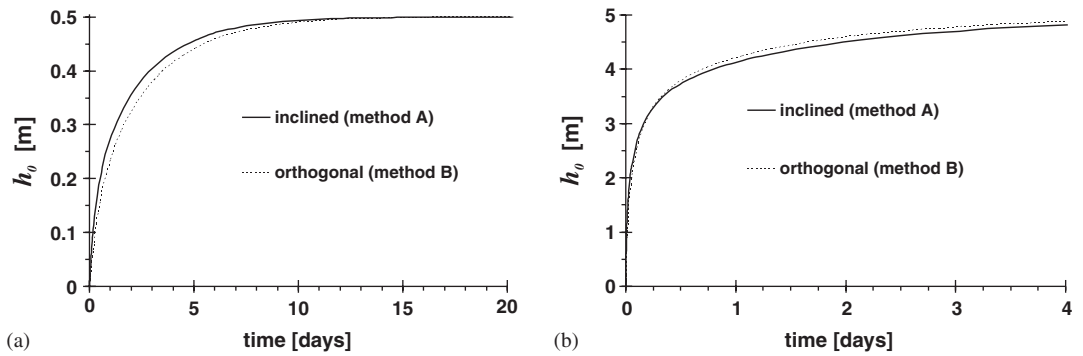

Figure 9. Transient hydraulic heads from (a) 2D and (b) 3D simulations using the initial condition $h_0(t=0)=0.0\,\text{m}$.

Simulated hydraulic heads for 2D transient flow match very well for both discretization methods (Figure 9(a)). However, Figure 9(a) suggests that method B slightly underestimates hydraulic heads. Underestimating hydraulic heads using method B is attributed to the longer flow path in the fracture, which delays the time to reach steady-state flow conditions.

For the 3D transient flow simulations, the simulated hydraulic heads are almost identical for both methods A and B (Figure 9(b)). However, method B slightly overestimates hydraulic heads. Note that method B underestimates hydraulic heads in 2D but slightly overestimates hydraulic heads in 3D. This result is intriguing and may be attributed to computer round-off errors. Further simulations (results not shown) have indicated that the difference is not due to flow boundary conditions, which are applied differently for the 2D and 3D simulations.

3.2. Solute transport simulations

All transport simulations presented below have been conducted using implicit transport time weighting and a steady flow field. The initial condition in 2D and 3D is $c(t=0)=0.0$.

Transport simulations for the 2D domain shown in Figure 8 indicate that concentrations obtained with method B do not match those from method A (Figure 10(a)). Method B systematically underestimates concentrations because the transport path in a fracture represented by orthogonal elements is lengthened. For orthogonal elements (method B), both transport path and fracture surface are greater by a factor equal to $\sqrt{2}$ compared with inclined triangulated elements (method A). The fracture permeability used for method B must be increased by a factor $\sqrt{2}$ to increase flow velocities and correct for the increased travel distance, such that

$$\kappa_{\text{fr}}^{\text{corr}} = \kappa_{\text{fr}} \cdot \sqrt{2} \tag{2}$$

Fracture permeability is given by $\kappa_{\text{fr}} = (2b)^2/12$ [48], and a corrected fracture aperture using orthogonal fracture elements is therefore

$$(2b)^{\text{corr}} = (2b) \cdot \sqrt{\sqrt{2}} \tag{3}$$

DOI: 10.1002/fld

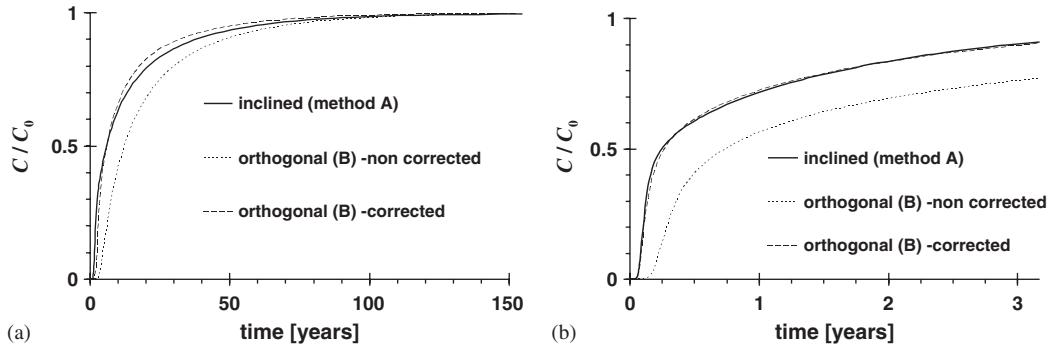

Figure 10. Concentrations from (a) 2D and (b) 3D simulations using the initial condition $c(t=0)=0.0$. Fracture aperture for orthogonal elements (method B) was corrected to match concentrations from method A.

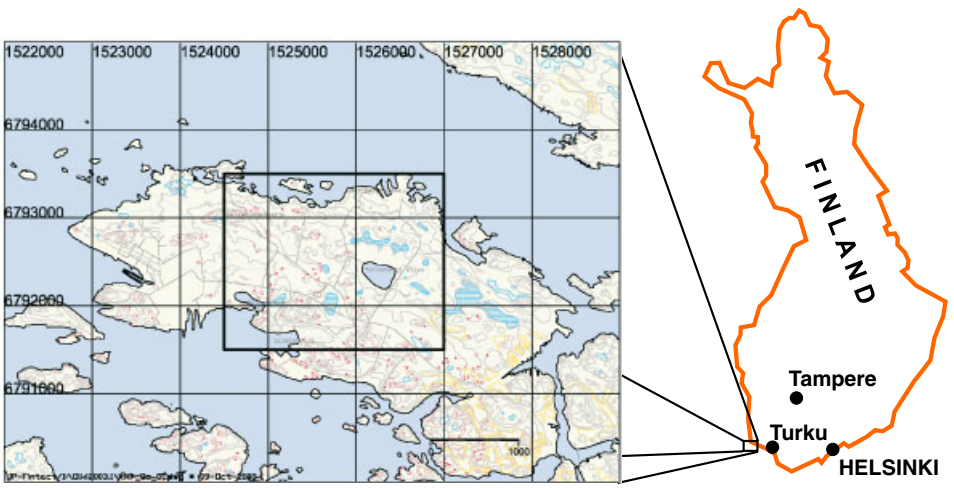

Figure 11. Olkiluoto Island in the Baltic Sea in southern Finland. The black frame on the left map shows the location of the repository for spent fuel.

The 2D transport simulation using orthogonal elements was repeated using a corrected fracture aperture $(2b)^{\text{corr}} = 59.46\,\mu\text{m}$. Results shown in Figure 10(a) demonstrate that with the corrected fracture aperture, method B matched results from method A.

The 3D transport simulations for the domain shown in Figure 5 also indicate that the longer fracture length for method B underestimates flow velocities. As a result, method B underestimates concentrations as shown in Figure 10(b). The 5669 orthogonal elements used for method B each have an area of size $0.02778\,\text{m}^2$, while the 3540 triangular elements for method A each have an area of size $0.02406\,\text{m}^2$. Therefore, in the 3D example, the fracture surface area for method B is 1.849 times greater than for method A. To adjust for the difference in fracture area, the corrected fracture permeability for method B must therefore be 1.848 times greater than the permeability

DOI: 10.1002/fld

Table IV. Characteristics of all fracture zones used for the field-scale example.

Fracture zone				
ID	Name	Fracture aperture (μm)	Fracture transmissivity (10^{-7} m^2 s^{-1})	Number of 2D elements
1	HZ001	25.9	0.13	928
2	HZ002	111.2	10.00	207
3	HZ003	95.4	6.31	140
4	HZ004	60.2	1.58	2820
5	HZ19A	129.7	15.85	6469
6	HZ008	239.6	100.00	2565
7	HZ19C	163.2	31.62	6894
8	HZ20A	221.9	79.43	7696
9	HZ20AE	111.2	10.00	331
10	HZ20B_ALT	163.2	31.62	7783
11	HZ21	27.9	0.16	7860
12	HZ21B	103.0	7.94	6823
13	BFZ099	27.9	0.16	7575

for method A, such that

$$\kappa_{\mathrm{fr}}^{\mathrm{corr}} = \kappa_{\mathrm{fr}} \cdot 1.848 \tag{4}$$

Accordingly, the corrected fracture aperture is

$$(2b)^{\mathrm{corr}} = (2b) \cdot \sqrt{1.848} \tag{5}$$

The 3D transport simulation using orthogonal elements was repeated using the corrected fracture aperture $(2b)^{\mathrm{corr}} = 67.99\,\mu\mathrm{m}$. Results shown in Figure 10(b) indicate very good agreement between results for methods A and B when the aperture is corrected.

4. FIELD-SCALE EXAMPLE: OLKILUOTO ISLAND, FINLAND

To illustrate the method presented in this paper, we simulated steady-state groundwater flow in crystalline rock at the Olkiluoto site, Finland, which is the proposed location for an underground spent fuel repository [49]. Olkiluoto is an island in the Baltic Sea, separated from the mainland by a narrow strait (Figure 11). Extensive site investigations have been carried out at Olkiluoto and spent fuel from the Finnish nuclear power plants will be disposed of in a repository located in the central part of the island (black frame on left map in Figure 11). The repository will be excavated in crystalline bedrock at a depth of 400–700 m below the level of the Baltic Sea.

A total of 31 deep open boreholes have been drilled at the site to monitor groundwater flow and hydraulic heads. Drilling reports of the boreholes revealed that the crystalline bedrock is slightly fractured, with an average fracture frequency of 1–3 fractures/m. Core sample studies revealed the presence of 13 major fracture zones (Table IV) acting as major hydraulic zones [49]. The geometry of each of these major zones is available as a series of triangular planes (as shown in Figure 1), which have been constructed from the intersection of the zones with the boreholes at depth. The

DOI: 10.1002/fld

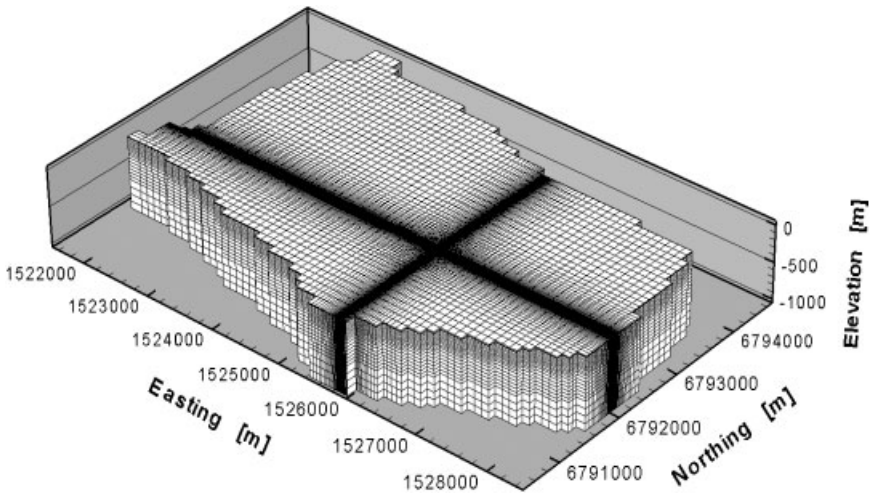

Figure 12. Locally refined irregular 3D grid with variable topography used for the field-scale example.

data used for the simulation presented here are obtained from the latest available hydrogeological model for the site [50].

A 3D grid was built to simulate steady-state groundwater flow observed at Olkiluoto Island (Figure 12). The grid consists of 198 792 3D hexahedral elements and 212 566 nodes. It has an irregular horizontal footprint and the elevation of the top layer of nodes represents either the island topography or sea level [49, 50]. Horizontal grid line spacing varies from 2 m near the boreholes to 100 m at the domain boundaries. Vertical grid line spacing varies from 10 m (domain top) to 100 m (domain bottom). Because fracture density is low, representing the fractures as discrete continua is given preference. Accordingly, the newly developed discretization method described here was used to represent the 13 undiscretized fracture zones (shown in Figure 13(a)) as discrete fractures in the grid. Figure 13(b) displays the discrete fractures and the total number of 2D fracture elements is 58 091 (Table IV). Spatial dimensions in Figure 13(a) and (b) are different because the undiscretized fracture zones (Figure 13(a)) extend outside the model area shown in Figures 12 and 13(b). Figure 13(b) also shows the location of 25 deep boreholes (KR01 ... KR16, KR19, KR20, KR22 ... KR28), which are represented as 1D line elements in the model.

The 3D rock matrix is assumed to be isotropic with a hydraulic conductivity value equal to $10^{-7}\,\mathrm{m\,s^{-1}}$ for $z>-50\,\mathrm{m}$ and $10^{-12}\,\mathrm{m\,s^{-1}}$ for $z<-50\,\mathrm{m}$. The aperture and transmissivity of the 2D hydraulic zones are variable and shown in Table IV. The radius of each well is 0.1 m, giving a well hydraulic conductivity value of $10^{4}\,\mathrm{m\,s^{-1}}$.

A first-type boundary condition is used for hydraulic heads at the top of the domain and the prescribed heads correspond to the interpolated groundwater table elevation on the island. Outside the island (lateral boundaries), the prescribed hydraulic head is equal to 0.0, which is the Baltic Sea elevation. The domain bottom is assumed to be impermeable.

Figure 14 shows the simulated steady-state head distribution in the fracture network. When available, the observed hydraulic head in deep boreholes was compared with the simulated hydraulic

DOI: 10.1002/fld

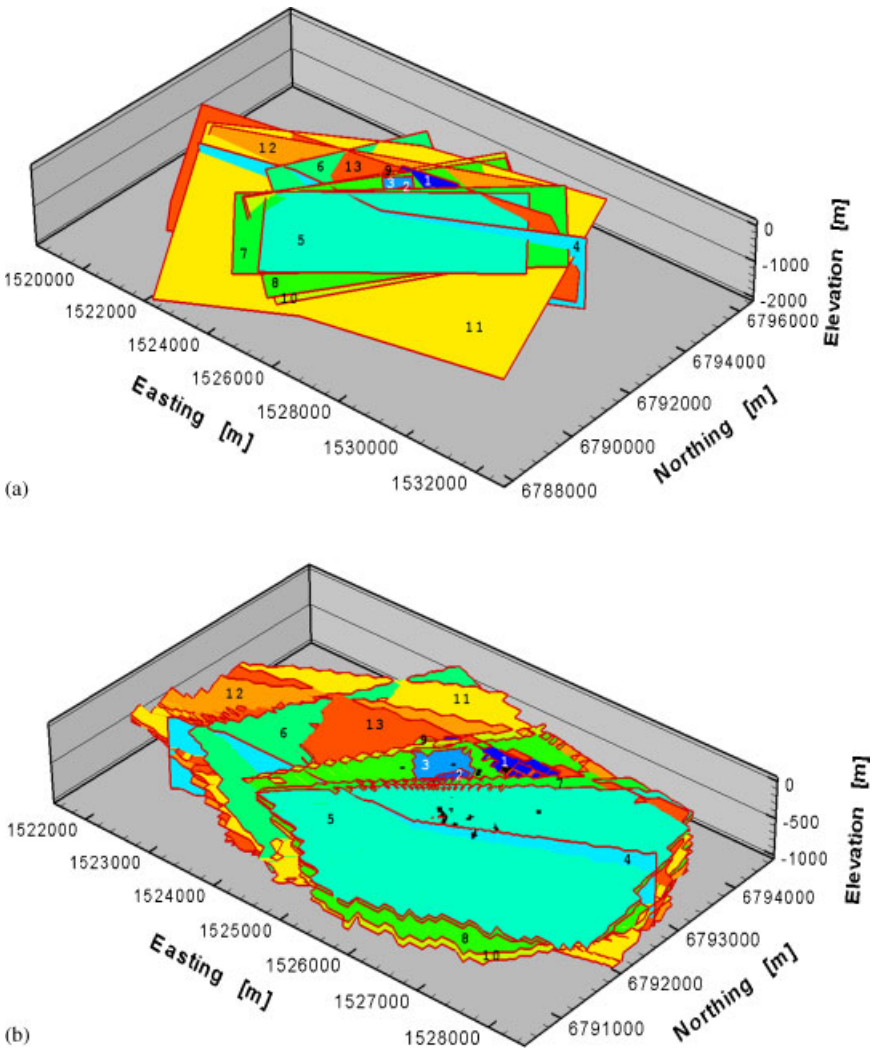

Figure 13. Fracture zones at the Olkiluoto site in Finland: (a) undiscretized triangulated zones where, for clarity, triangle edges are not shown and (b) discretized triangulated zones and boreholes (black dots). Spatial dimensions of the two plots are different because the undiscretized zones shown in (a) cover an area larger than the model area shown in (b). However, perspective and axes ratios are identical to allow easy comparison.

head and the comparison is shown in Figure 15. Note that the purpose of this simulation is to apply the new fracture discretization method to a field-scale example. The goal is not to calibrate the model and, therefore, simulated heads shown in Figure 15 are for an uncalibrated model. Accordingly, the figure does not show good but approximate agreement between observed and simulated hydraulic head.

DOI: 10.1002/fld

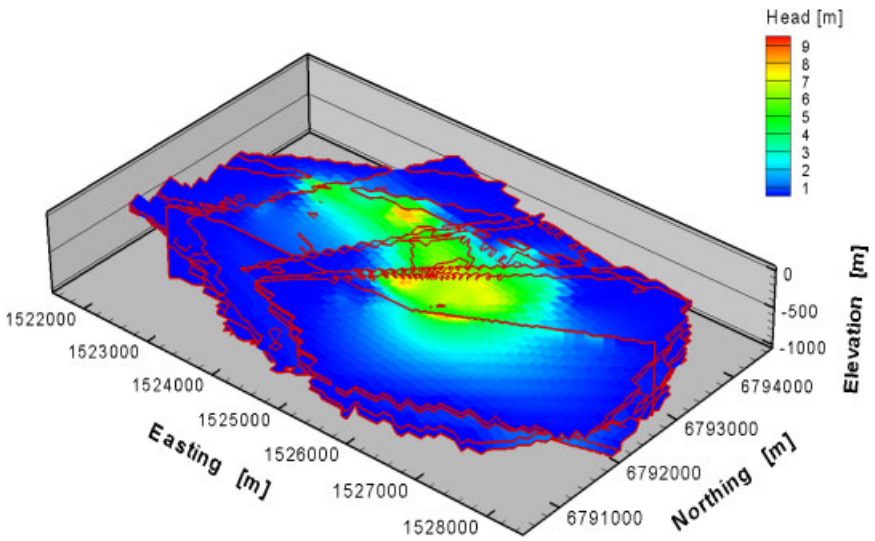

Figure 14. Steady-state hydraulic heads in the fracture network.

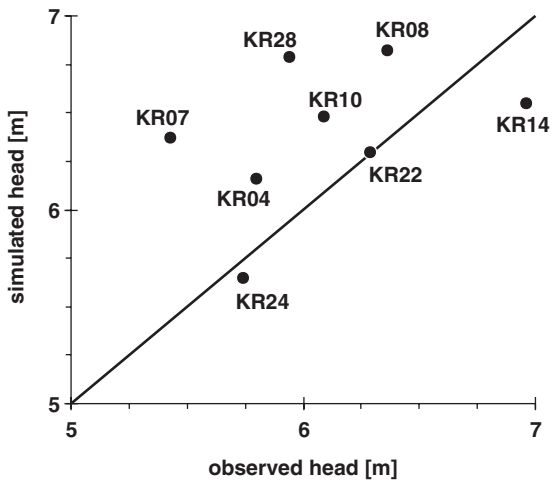

Figure 15. Observed *versus* simulated steady-state hydraulic heads in open boreholes at the Olkiluoto site.

5. SUMMARY AND CONCLUSIONS

This study presents a new technique to represent inclined non-planar fractures by a set of 2D horizontal/vertical/inclined triangular/rectangular fracture elements in a 3D irregular grid. The technique (i) assumes a triangulated natural fracture, (ii) determines 3D element edge intersections

DOI: 10.1002/fld

for each triangle, (iii) moves intersections to closest nodes and (iv) chooses 2D triangular and rectangular fracture elements to finally discretize the continuous non-planar fracture.

The new technique was implemented in the FRAC3DVS model. The enhanced model was then used to conduct flow and transport simulations in 2D and 3D, where an inclined fracture is discretized with inclined triangular elements. The simulations were repeated with the inclined fracture being discretized with orthogonal rectangular elements and the two sets of simulations were compared. In summary, the simulations indicate that:

(1) For 2D transient flow simulations, inclined fractures have to be discretized with inclined elements because orthogonal elements underestimate hydraulic heads (using $h_0(t=0)=0.0\,\mathrm{m}$).
(2) For 2D/3D steady-state flow and transient 3D flow simulations, inclined fractures can be discretized with inclined or orthogonal elements. Both discretizations give identical flow results.
(3) For 2D/3D transport simulations, inclined fractures have to be discretized with inclined elements because orthogonal elements significantly underestimate concentrations (using $c(t=0)=0.0$).
(4) Results of 2D/3D transport simulations using inclined and orthogonal elements are identical when the permeability of the orthogonal fracture elements is multiplied by the ratio of the fracture surface areas using

$$\kappa_{\mathrm{fr}}^{\mathrm{corr}} = \kappa_{\mathrm{fr}} \cdot \frac{A_{\mathrm{fr}}^{\mathrm{orthogonal}}}{A_{\mathrm{fr}}^{\mathrm{inclined}}} \tag{6}$$

Because fracture permeability is calculated with $\kappa_{\mathrm{fr}} = (2b)^2/12$, the corrected fracture aperture using orthogonal fracture elements is

$$(2b)^{\mathrm{corr}} = (2b) \cdot \sqrt{\frac{A_{\mathrm{fr}}^{\mathrm{orthogonal}}}{A_{\mathrm{fr}}^{\mathrm{inclined}}}} \tag{7}$$

The enhanced model was used to discretize a realistic network of non-planar fractures and to conduct steady-state flow simulations at the field scale. The simulated domain corresponds to fractured crystalline bedrock on the Olkiluoto island, Finland. It has been shown that the new discretization method accurately represents fracture zones in the numerical grid, which demonstrates flexibility and robustness of the new method. With an uncalibrated model, observed hydraulic heads could be approximately reproduced, showing that the proposed discretization procedure offers new possibilities to simulate flow and has great potential to simulate transport in complex 3D fracture networks.

NOMENCLATURE

The use of symbols for main variables is consistent throughout the entire text. The mathematical symbols used in this paper correspond to those used by Graf and Therrien [19] and are not listed here.

DOI: 10.1002/fld

ACKNOWLEDGEMENTS

We thank Ontario Power Generation (OPG) as well as the Natural Sciences and Engineering Research Council of Canada (NSERC) for financial support of this project. Thanks are also due to Stefano Normani (University of Waterloo) for providing orthogonal elements of discretized inclined fractures and to Posiva Oy for kind permission to use data from the Olkiluoto site. The constructive comments of Jean-Michel Lemieux and an anonymous reviewer are greatly appreciated and have helped improve the paper.

REFERENCES

1. Long JCS, Remer JS, Wilson CR, Witherspoon P. Porous media equivalents for networks of discontinuous fractures. *Water Resources Research* 1982; **18**(3):645–658.
2. Smith L, Schwartz FW. An analysis of the influence of fracture geometry on mass transport in fractured media. *Water Resources Research* 1984; **20**(9):1241–1252.
3. Andersson J, Dverstorp B. Conditional simulations of fluid flow in three-dimensional networks of discrete fractures. *Water Resources Research* 1987; **23**(10):1876–1886.
4. Cacas M-C, Ledoux E, de Marsily G, Tillie B, Barbreau A, Durand E, Fuega B, Peaudecerf P. Modeling fracture flow with a stochastic discrete fracture network: 1. The flow model. *Water Resources Research* 1990; **26**(3):479–489.
5. Cacas M-C, Ledoux E, De Marsily G, Barbreau A, Calmels P, Gaillard B, Margritta R. Modeling fracture flow with a stochastic discrete fracture network: 2. The transport model. *Water Resources Research* 1990; **26**(3):491–500.
6. Long JCS, Karasaki K, Davey A, Peterson J, Landsfeld M, Kemeny J, Martel S. An inverse approach to the construction of fracture hydrology models conditioned by geophysical data. *International Journal of Rock Mechanics and Mining Sciences* 1991; **28**(2/3):121–142.
7. Dverstorp B, Andersson J, Nordqvist W. Discrete fracture network interpretation of field trace migration in sparsely fractured rock. *Water Resources Research* 1992; **28**(9):2327–2343.
8. Nordqvist AW, Tsang YW, Tsang CF, Dverstorp B, Andersson J. A variable aperture fracture network model for flow and transport in fractured rocks. *Water Resources Research* 1992; **28**(6):1703–1713.
9. Sudicky EA, McLaren RG. The Laplace transform Galerkin technique for large-scale simulation of mass transport in discretely-fractured porous formations. *Water Resources Research* 1992; **28**(2):499–514.
10. Ezzedine S. Study of transient flow in hard fractured rocks with a discrete fracture network model. *International Journal of Rock Mechanics and Mining Sciences* 1993; **30**(7):1605–1609.
11. Dershowitz WS, Miller I. Dual porosity fracture flow and transport. *Geophysical Research Letters* 1995; **22**(11):1441–1444.
12. Watanabe K, Takahashi H. Fractal geometry characterization of geothermal reservoir fracture networks. *Journal of Geophysical Research* 1995; **100**(B1):521–528.
13. Herbert AW. Modelling approaches for discrete fracture network flow analysis. In *Coupled Thermo-Hydro-Mechanical Processes of Fractured Media*, Stephansson O, Jing L, Tsan C-F (eds), vol. 79. Elsevier: Amsterdam, 1996; 213–229.
14. Therrien R, Sudicky EA. Three-dimensional analysis of variably saturated flow and solute transport in discretely-fractured porous media. *Journal of Contaminant Hydrology* 1996; **23**(6):1–44.
15. Azevedo IC, Vaz LE, Vargas EA. Numerical procedure for the analysis of the hydromechanical coupling in fractured rock masses. *International Journal for Numerical and Analytical Methods in Geomechanics* 1998; **22**(11):867–901.
16. Shikaze SG, Sudicky EA, Schwartz FW. Density-dependent solute transport in discretely-fractured geologic media: is prediction possible? *Journal of Contaminant Hydrology* 1998; **34**(10):273–291.
17. Woodbury A, Zhang KN. Lanczos method for the solution of groundwater flow in discretely fractured porous media. *Advances in Water Resources* 2001; **24**(6):621–630.
18. Wang EZ, Yue ZQ, Tham LG, Tsui Y, Wang HT. A dual fracture model to simulate large-scale flow through fractured rocks. *Canadian Geotechnical Journal* 2002; **39**:1302–1312.
19. Graf T, Therrien R. Variable-density groundwater flow and solute transport in porous media containing nonuniform discrete fractures. *Advances in Water Resources* 2005; **28**(12):1351–1367.
20. Graf T, Therrien R. Variable-density groundwater flow and solute transport in irregular 2D fracture networks. *Advances in Water Resources* 2007; **30**(3):455–468.

DOI: 10.1002/fld

21. Graf T, Therrien R. Coupled thermohaline groundwater flow and single-species reactive solute transport in fractured porous media. *Advances in Water Resources* 2007; **30**(4):742–771.
22. Herget G. *Stresses in rock*. SWETS: Ottawa, Canada, 17.
23. Long JCS, Billaux DM. Use of geostatistics to incorporate spatial variability in the modeling of flow through fracture networks. *Report Number LBL-21439*, Lawrence Berkeley Laboratory, Berkeley, CA, U.S.A., 1986; 93.
24. Long JCS, Billaux DM. From field data to fracture network modeling: an example incorporating spatial structure. *Water Resources Research* 1987; **23**(7):1201–1216.
25. Isaaks EH, Srivastava RM. *An Introduction to Applied Geostatistics*. Oxford University Press: New York, NY, U.S.A., 1990; 592.
26. Priest SD. *Discontinuity Analysis for Rock Engineering*. Chapman & Hall: London, U.K., 1993; 47.
27. Shimizu A, Hashida T, Watanabe K, Willis-Richard J. New development of 3-D stochastic model for design of HDR/HWR geothermal reservoirs system. *Proceedings of the World Geothermal Congress*, Kyushu-Tohoku, Japan, 28 May–10 June, 2000; 3877–3882.
28. Tezuka K, Watanabe K. Fracture network modeling of Hijiori hot dry rock reservoir by deterministic and stochastic crack network simulator (D/SC). *Proceedings of the World Geothermal Congress*. Kyushu–Tohoku, Japan, 28 May–10 June, 2000; 3933–3938.
29. Dverstorp B, Andersson J. Application of the discrete fracture network concept with filed data: possibilities of model calibration and validation. *Water Resources Research* 1989; **25**:540–550.
30. Billaux DM. Hydrogéologie des milieux fracturés. Géométrie, connectivité et comportement hydraulique. *Ph.D. Thesis*, *École Nationale Supérieure des Mines de Paris*, Document of the BRGM 186, Orléans, France, 1990.
31. Dershowitz WS, LaPointe P, Einstein HH, Ivanova V. Fractured reservoir discrete feature network technologies. A project of fundamental geoscience research and development. *DOE Contract G4S51728*. Golder Associates Inc.: Redmond, WA, U.S.A., 1997.
32. Yu Q. Analyses for fluid flow and solute transport in discrete fracture network. *Ph.D. Thesis*, Department of civil engineering, Kyoto University, Kyoto, Japan, 2000; 161.
33. FracMan technology group, 2002. Available from: http://fracman.golder.com.
34. Golder Associates Inc. FracWorks XP discrete feature simulator, user documentation version 4.0. Golder Associates Inc., Redmond, WA, U.S.A., 2004; 88.
35. Mustapha H. Simulation numérique de l'écoulement dans des milieux fracturés tridimensionnels. *Ph.D. Thesis*, Université de Rennes, Rennes, France, 2005; 151. Available from: http://www.irisa.fr/sage/jocelyne/.
36. Mustapha H, Beaudoin A, Erhel J, De Dreuzy JR. Parallel simulations of underground flow in porous and fractured media. *International Conference on Parallel Computing*, *ParCo'2005*, Malaga, Spain, September 2005.
37. Bruines PA. Laminar ground water flow through stochastic channel networks in rock. *Ph.D. Thesis*, École Polytechnique Fédérale de Lausanne, Lausanne, Switzerland, 2003; 152. Available from: http://biblion.epfl.ch/EPFL/theses/2003/2736/EPFL_TH2736.pdf.
38. Moenickes S, Taniguchi T, Kaiser R, Zielke W. A 2.75D finite element model of 3D fracture network systems. *Proceedings of the 11th International Meshing Roundtable*, Ithaca, NY, U.S.A., September 2002, Sandia National Laboratories, 2002; 161–168.
39. Krasovec ML, Burns DR, Willis ME, Chi S, Toksöz MN. 3-D finite difference modeling for borehole and reservoir applications. *Earth Resources Laboratory Department of Earth*, *Atmospheric*, *and Planetary Sciences Massachusetts Institute of Technology*, Cambridge, MA, U.S.A., 2004; 15.
40. Normani SD, Sykes JF, Sudicky EA, Park Y-J. Palaeo-evolution and uncertainty analysis of regional groundwater flow in discretely fractured crystalline rock. In *Calibration and Reliability in Groundwater Modelling*: *From Uncertainty to Decision Making*, *Proceedings of ModelCARE'2005*, Bierkens MFP, Gehrels JC, Kovar K (eds), The Hague, Netherlands, June 2005. IAHS Publication No. 304, ISBN 1-901502-58-9, 2006; 180–186.
41. Castaing C, Chilès JP, Genter A, Bourgine B. Geometrical fracture modelling. In *Fracture Interpretation and Flow Modelling in Fractured Reservoirs*, Chapter 3, Bech N *et al*. (eds). 2001; 33–46.
42. Beaudoin G, Therrien R, Savard C. 3D numerical modelling of fluid flow in the Val-d'Or orogenic gold district: major crustal shear zones drain fluids from overpressured vein fields. *Mineralium Deposita* 2006; **41**(1):82–98.
43. Therrien R, McLaren RG, Sudicky EA, Panday SM. *HYDROGEOSPHERE—A Three-Dimensional Numerical Model Describing Fully-Integrated Subsurface and Surface Flow and Solute Transport*. Université Laval, University of Waterloo, 2004; 275.
44. Srivastava RM. Personal communication, 2006.
45. Istok J. *Groundwater Modeling by the Finite Element Method*. American Geophysical Union: Washington, DC, U.S.A., 495.

DOI: 10.1002/fld

46. Ogata A, Banks RB. A solution of the differential equation of longitudinal dispersion in porous media. US Geological Survey. *Technical Report 411-A*, Professional Paper, 1961.
47. Tang DH, Frind EO, Sudicky EA. Contaminant transport in fractured porous media: analytical solution for a single fracture. *Water Resources Research* 1981; **17**(3):555–564.
48. Bear J. *Hydraulics of Groundwater*. McGraw-Hill: New York, NY, U.S.A., 567.
49. Vaittinen T, Ahokas H, Heikkinen E, Hellä P, Nummela J, Saksa P, Tammisto E, Paulamäki S, Paananen M, Front K, Kärki A. Bedrock model of the Olkiluoto site, version 2003/1. *Working Report 2003-43*, Eurajoki, Finland, Posiva Oy, 2003; 266.
50. Ahokas H, Vaittinen T, Tammisto E, Nummela J. Compilation of the hydrogeological model of Olkiluoto, version 2006. *Working Report 2007-01*, Posiva Oy, 2007.

DOI: 10.1002/fld